Aeromagnetic Compensation Algorithm Based on Calibration of Fluxgate Measurements

Dehua Liu[1], Changping Du[2], and Mingyao Xia[2]
[1] University of Electronic Science and Technology of China, Chengdu 611731, China
[2] Peking University, Beijing 100871, China
andyuestc@std.uestc.edu.cn, myxia@pku.edu.cn

Abstract—This paper discusses about a combined method of tri-axial fluxgate parameter calibration scheme and aeromagnetic compensation algorithm. The aircraft's magnetic interference is a bottle-neck factor in obtaining high quality aeromagnetic data. According to Tolles-Lawson model, the accuracy of aircraft's directional cosines directly affects compensation quality. In this paper, a method of calibrating the fluxgate magnetometer is introduced and then the calibration parameters obtained is used to aeromagnetic survey. With the help of calibrated fluxgate magnetometer, an iterative aeromagnetic compensation algorithm is developed to enhance the ordinary aeromagnetic compensation method. Simulated experimental results show that the proposed scheme is viable to improve the compensation accuracy.

Keywords—Aeromagnetic compensationt; Tolles-Lawson model; iteration method; trust region method

I. INTRODUCTION

It is well known that aeromagnetic compensation plays a vital role in aeromagnetic survey because of the intractable interference generated by the aircraft [1]. The measured signal should be compensated to eliminate the magnetic interference caused by the aircraft in practical engineering, as the magnetic interference can easily overwhelm target signal, which is related to flight direction, attitude maneuver, and magnetic material in aircraft. There are two kinds of historical methods for solving the problem [2], one of which is to construct linear equations by modeling the interference based on Tolles-Lawson model. In 1950, Tolles and Lawson [3] proposed that the magnetic interference consists of permanent, induced, and eddy-current fields, which is based on the hypothesis that geomagnetic field is even and stable; compensation parameters are invariant due to rigidly connected aircraft structure. Researchers are mostly focused on compensation parameters' solving algorithm based on the Tolles-Lawson equations or add interference terms according to actual requirements [4], as Tolles-Lawson model is efficiently to eliminate the magnetic interference. The other method of compensating the interference is to construct a neural network model without regard to physical principles, which directly output value of interference estimated by input data [5].

The scalar magnetometer and tri-axial fluxgate sensor are commonly used as the measuring instruments in aeromagnetic compensation. Scalar magnetometer is applied to measure the total magnetic field, and the directional cosine in Tolles-Lawson equations is determined by the measurements of tri-axial fluxgate magnetometer. The errors of instruments immediately affect the precision in aeromagnetic compensation [6]. Scalar magnetometer with accuracy down to 0.01nT is generally reliable, while the tri-axial fluxgate magnetometer with accuracy of 0.1nT has a poor precision in comparison to scalar magnetometer. The precision is able to satisfy the requirement for calculation of directional cosines. However, there exist non-orthogonality and zero-biases in fluxgate magnetometer, which is an obstacle interfering the improvement of compensation precision. Some researchers have proposed some methods to calibrate fluxgate's measurements before using them to calculate the directional cosines. The purpose of this paper is to present a method to calibrate fluxgate measurements, both on tri-axial orthogonality and zero-biases, in order to enhance the accuracy of compensation.

II. METHOD

A. Calibration for Tri-axial Fluxgate

The errors of a tri-axial fluxgate result from three aspects: non-orthogonality of its three axes, sensitivities in three directions, and zero-biases of its three components. Hence, the actual magnetic field at fluxgate position may be expressed as:

$$\mathbf{B}_{\text{flu}} = \mathbf{STH}_{\text{m}} + \mathbf{d} \tag{1}$$

where $\mathbf{H}_{\text{m}}$ is the measured magnetic field by the tri-axial fluxgate, $\mathbf{S}$ stands for a sensitivity matrix, $\mathbf{T}$ is the transform matrix from the non-orthogonal fluxgate frame to the orthogonal aeromagnetic TLV frame, and $\mathbf{d}$ reflects the zero-biases. They are written as:

$$\mathbf{S} = \begin{bmatrix} S_x & 0 & 0 \\ 0 & S_y & 0 \\ 0 & 0 & S_z \end{bmatrix}, \ \mathbf{T} = \begin{bmatrix} T_{11} & 0 & T_{13} \\ T_{21} & 1 & T_{23} \\ T_{31} & 0 & T_{33} \end{bmatrix}, \ \mathbf{d} = \begin{bmatrix} d_1 \\ d_2 \\ d_3 \end{bmatrix} \tag{2}$$

where it has been assumed that the Y-axis of the non-orthogonal fluxgate frame and the L-axis of the aeromagnetic TLV frame is coincident, and $T_{11}^2 + T_{21}^2 + T_{31}^2 = T_{13}^2 + T_{23}^2 + T_{33}^2 = 1$ is required; thus, there is only four degrees of freedom in $\mathbf{T}$. By letting $\mathbf{W} = \mathbf{ST}$, we obtain the calibrated magnetic field as

$$\mathbf{B}_{\text{flu}} = \mathbf{WH}_{\text{m}} + \mathbf{d} \tag{3}$$

where $\mathbf{W}$ is a transform matrix with seven degrees of freedom:

$$\mathbf{W} = \begin{bmatrix} w_{11} & 0 & w_{13} \\ w_{21} & w_{22} & w_{23} \\ w_{31} & 0 & w_{33} \end{bmatrix}. \quad (4)$$

The objective function for calibration of the tri-axial fluxgate is

$$\mathrm{E}(\mathbf{W},\mathbf{d}) = \arg\min_{\mathbf{W},\mathbf{d}} \left(\left| \mathbf{B}_{\mathrm{flu}} \right| - B_{\mathrm{opt}} \right) \quad (5)$$

where B_{opt} is the measurement values by the scalar optical-pumping magnetometer. The optimization problem (5) can be converted as a constrained nonlinear optimization problem, which may be solved by using the trust region method [7]. Once the parameters $\mathbf{W}$ and $\mathbf{b}$ are found, the magnetic field is calculated by (3), and the directional vector is obtained by

$$\mathbf{u} = \mathbf{B}_{\mathrm{flu}} / \left| \mathbf{B}_{\mathrm{flu}} \right|. \quad (6)$$

This calibrated directional vector will be utilized to replace $\mathbf{u} = \mathbf{H}_{\mathrm{m}} / \left| \mathbf{H}_{\mathrm{m}} \right|$ that is used in the conventional compensation method.

B. Aeromagnetic Compensation

According to Tolles-Lawson model [3], the maneuvering interference of the aircraft consists of three parts: the permanent interference caused by the residue magnetization, the induced interference caused by temporal magnetization of ferrous material, and the eddy-current interference caused by time-varying ambient magnetic fields. The total inference is written as

$$B_d = \sum_{i=1}^{3} a_i u_i + B_g \sum_{i=1}^{3} \sum_{j=i}^{3} b_{ij} u_i u_j + \sum_{i=1}^{3} \sum_{j=1}^{3} c_{ij} (B_g \dot{u}_i + \dot{B}_g u_i) u_j \quad (7)$$

where B_g is the ambient magnetic field, $\dot{B}_g = dB_g / dt$, and $\dot{u}_i = du_i / dt$ with u_i already obtained by (6). There are a total of 18 coefficients in (7). What measured by an optical-pumping magnetometer is the superposition of the ambient field and interfering field, i.e., $B_{\mathrm{opt}} = B_g + B_d$. Hence, the objective function for extracting the compensation coefficients is

$$\mathrm{E}(\mathbf{a},\mathbf{b},\mathbf{c}) = \arg\min_{\mathbf{a},\mathbf{b},\mathbf{c}} \left(B_{\mathrm{opt}} - B_g - B_d \right) \quad (8)$$

This is an indefinite optimization problem unless the ambient field B_g has been given, which is, unfortunately, not known in prior.

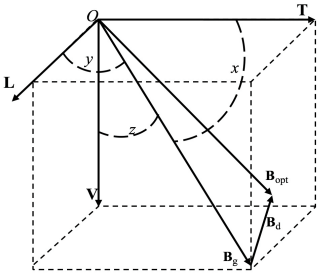

Fig. 1. Reference frame used in aeromagnetic compensation.

To proceed, we assume that B_g is slowly varying, so that it may be estimated from B_{opt} by using a low-pass filter, i.e.

$$B_g \approx \text{low-pass-filtering}(B_{\mathrm{opt}}) = \tilde{B}_g \quad (9)$$

where the upper cutoff frequency may be set to be 0.1 Hz. On the other hand, the interference field B_d is dominatingly band-limited, so that it may be estimated by using a band-pass filter, i.e.

$$B_d \approx \text{band-pass-filtering}(B_{\mathrm{opt}}) = \tilde{B}_d \quad (10)$$

where the lower and upper cutoff frequencies may be set to 0.1 Hz and 0.2 Hz, respectively. Now, substituting (9) and (10) into (7) and processing the right-hand side of (7) using the same band-pass filter, an optimized solution for the 18 compensation coefficients can be found through

$$\mathrm{E}(\mathbf{a},\mathbf{b},\mathbf{c}) = \arg\min_{\mathbf{a},\mathbf{b},\mathbf{c}} \left(\tilde{B}_d - \hat{B}_d \right) \quad (11)$$

where $\tilde{B}_d$ is given by (10), and $\hat{B}_d$ is the result after band-pass filtering of the right-hand side of (7) with B_g given by (9) in place. Then, with the obtained coefficients, the interfering magnetic field is calculated by (7), denoted as $\tilde{B}_d'$, and the ambient magnetic field is retrieved by $\tilde{B}_g' = B_{\mathrm{opt}} - \tilde{B}_d'$. These ambient field $\tilde{B}_g'$ and interfering field $\tilde{B}_d'$ can be compared with (9) and (10), respectively. If the comparison is unsatisfactory, we may let $B_g \approx (\tilde{B}_g + \tilde{B}_g')/2$ and $B_d \approx (\tilde{B}_d + \tilde{B}_d')/2$ to replace the estimates of (9) and (10), and substituting them into (7) to find a better set of compensation coefficients.

III. SIMULATION EXPERIMENT

In order to verify the effect of compensation algorithm based on the calibrated fluxgate data, some simulation experiments are designed. In the experiments, the background magnetic field B_g comes from real measured data in Beijing suburbs and the fluxgate data $\mathbf{H}_{\mathrm{m}}$ to describe the aircraft's maneuvers comes from a real aeromagnetic compensation experiment. During the tests, the platform performs roll, pitch and yaw maneuvers on each direction of the four headings [9]. The sampling frequency of both the scalar magnetometer and the vector fluxgate is 10 Hz. The magnetic interferences, including the permanent, induced, and eddy-current components, are simulated using assumed compensation coefficients. That is, the magnetic interference measured by the optical-pumping magnetometer is taken to be $B_{\mathrm{opt}} = B_g + B_d$, where B_d is calculated by (7) with given coefficients $\{\mathbf{a},\mathbf{b},\mathbf{c}\}$ and $\{\mathbf{u}\}$ found by (6).

A series of offset parameters are used to stimulate the measurements of the fluxgate sensor. A typical set of offset parameters are shown in Table I. The "given" parameters are used to obtain the "true" fluxgate data by (3), the "true" directional cosines by (6), and the "true" interferences by (7). Then the proposed calibration algorithm of (5) is executed to

retrieve the "given" parameters as list by "solved" in Table I. It can be seen that the accuracy for the orthogonality elements of **W** is better than 3%, while that for the zero-biases **d** is better than 8%.

The calibrated results for the directional cosines ($\cos X = u_1$, $\cos Y = u_2$, $\cos Z = u_3$) and total field ($|\mathbf{B}_{\text{flu}}|$) are shown in Fig. 2. It is seen that the calibration for $\cos Z$ is appreciable, and the calibration for total field is very satisfying. Once the calibration is finished, the compensation algorithm using (9)-(11) is performed. The found coefficients $\{\mathbf{a}, \mathbf{b}, \mathbf{c}\}$ can be compared with their assumed values, or the compensated optical-pumping data can be compared with the "true" or "real" values. As shown in Fig. 3, the compensated result by using the calibrated fluxgate data is in very agreement with the real data, almost completely overlapped, where a band-pass filtering with bandwidth from 0.06 Hz to 0.6 Hz has been applied.

Last, analyses of compensation effects with varying offset parameters **w** and **d** are conducted. The parameters of w_{ij} for $i \neq j$ are set to be from -0.1 to 0.1, and for $i = j$ are set to be from 0.9 to 1.1. The zero-biases for d_i ($i = 1,2,3$) are set to be from -200 nT to 200 nT. The standard deviation (std) of the compensated data (the green line in Fig. 3) is used to measure the compensation quality. Fig. 4 show the typical results, where the changes of std with w_{11} and d_3 are plotted, respectively. It is seen that the calibration effects are significant. The changes of std with other w_{ij} are almost the same as with w_{11}, and the changes of std with other d_i are almost the same as with d_3.

TABLE I. THE GIVEN PARAMETERS AND SOLVED PARAMETERS

	w_{11}	w_{13}	w_{21}	w_{22}	w_{23}
Given	0.93	0.04	-0.04	0.92	-0.05
Solved	0.9254	0.0362	-0.0431	0.9182	-0.0491
	w_{31}	w_{33}	d_1	d_2	d_3
Given	0.04	1.08	160	280	-230
Solved	0.0621	1.0847	170.4302	302.5774	-245.9947

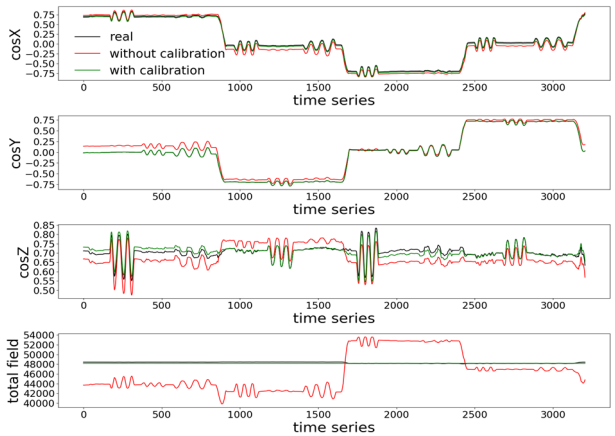

Fig. 2. The directional cosines and total field with and without calibration. The red curve represents the data without calibration. The green curve represents the data with calibration. The black curve represents the real data.

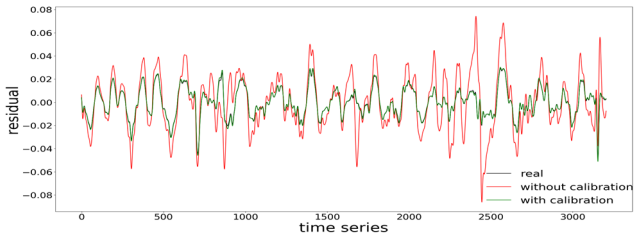

Fig. 3. Residual compensated signal after band-pass filtering within 0.06~0.6 Hz. The red curve represents residual without calibration. The green represents residual with calibration.

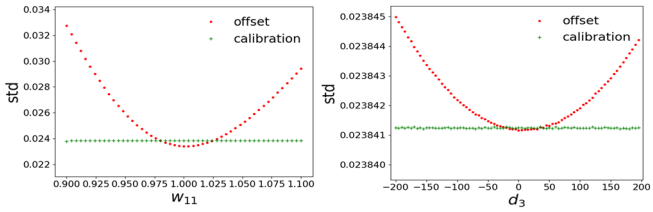

Fig. 4. The variations of standard deviation of residual signals with the orthogonal parameters w_{11} and zero-biases d_3.

IV. CONCLUSION

Non-orthogonality and zero-biases of tri-axial fluxgate magnetometer can be obstacles to improve the aeromagnetic compensation accuracy. This work presents a procedure to retrieve the non-orthogonal and zero-bias parameters by using the trust region method, and then obtain calibrated fluxgate data. Simulation experiments show that the calibration methods are viable if the separation between the fluxgate and optical-pumping magnetometers is small so that the interferences produced by the platform at the two positions can be taken to be the same.

Acknowledgment: This work is supported by NSFC under Project 61531001.

REFERENCES

[1] Z. Chang-Da, "Airborne tensor magnetic gradiometry——the latest progress of airborne magnetometric technology[J]," *Chinese Journal of Engineering Geophysics,* vol. 5, p. 007, 2006.

[2] M. N. Nabighian *et al.*, "The historical development of the magnetic method in exploration," *Geophysics,* vol. 70, no. 6, pp. 33ND-61ND, 2005.

[3] W. Tolles and J. Lawson, "Magnetic compensation of MAD equipped aircraft," *Airborne Instruments Lab. Inc., Mineola, NY, Rept,* pp. 201-1, 1950.

[4] S. H. Bickel, "Small signal compensation of magnetic fields resulting from aircraft maneuvers," *IEEE Transactions on aerospace and electronic systems,* no. 4, pp. 518-525, 1979.

[5] P. M. Williams, "Aeromagnetic compensation using neural networks," *Neural Computing & Applications,* vol. 1, no. 3, pp. 207-214, 1993.

[6] R. Groom, R. Jia, and B. Lo, "Magnetic compensation of magnetic noises related to aircraft's maneuvers in airborne survey," in *Symposium on the Application of Geophysics to Engineering and Environmental Problems 2004*, 2004, pp. 101-108: Society of Exploration Geophysicists.

[7] R. H. Byrd, J. C. Gilbert, and J. Nocedal, "A trust region method based on interior point techniques for nonlinear programming," *Mathematical Programming,* vol. 89, no. 1, pp. 149-185, 2000.

[8] G. Noriega, "Performance measures in aeromagnetic compensation," *The Leading Edge,* vol. 30, no. 10, pp. 1122-1127, 2011.

[9] B. Gu, Q. Li, and H. Liu, "Aeromagnetic compensation based on truncated singular value decomposition with an improved parameter-choice algorithm," in *Image and Signal Processing (CISP), 2013 6th International Congress on*, 2013, vol. 3, pp. 1545-1551.